Ab-initio modeling of protein/biomaterial interactions: influence of amino acid polar side chains on adsorption at hydroxyapatite surfaces

Ab-initio modeling of protein/biomaterial interactions: influence of amino acid polar side chains on adsorption at hydroxyapatite surfaces

Albert Rimola[a, b], Marta Corno[b], Jorge Garza[c] and Piero Ugliengo[b*]

[a]Departament de Química, Universitat Autònoma de Barcelona, Bellaterra 08193, Spain. [b]Dipartimento di Chimica IFM, NIS Centre of Excellence and INSTM (Materials Science and Technology National Consortium), Università di Torino, Via P. Giuria 7, 10125 Torino, Italy. [c]Universidad Autónoma Metropolitana Iztapalapa, Departamento de Química, División de Ciencias Básicas e Ingeniería. Distrito Federal. 09340, México

*Corresponding author. E-mail: piero.ugliengo@unito.it

Abstract

The adsorption from gas-phase of five different amino acids (AA), namely Gly, Ser, Lys, Gln and Glu, on three surface models of hexagonal hydroxyapatite (HA) has been studied at B3LYP level with Gaussian type basis set within a periodic approach. The AA adsorption was simulated on the (001) and (010) stoichiometric surfaces, the latter both in its pristine and water reacted form. Low/high AA coverage has been studied by doubling the HA unit cell size. The AA have been docked to the HA surfaces following the electrostatic complementarity between the electrostatic potentials of AA and the bare HA. Gly adsorbs as a zwitterion at the (001) surface, whereas at the (010) ones the proton of the COOH group is transferred to the surface resulting in an HA^{+}/Gly^{-} ion pair. For the other AA the common COOH-CH-NH_2 moiety behaves like in Gly, while the specific side-chain functionalities adsorb at the HA surfaces by maximizing electrostatic and H-bond interactions. The interactions between the side chains and the HA surface imparts a higher stability compared to the Gly case, with Glu being the strongest adsorbate due to its high Ca affinity and H-bond donor propensity. For AA of large size, the adsorption is more favorable in conditions of low coverage as repulsion between adjacent AA is avoided. For all considered AA, the strongest interaction is always established on the (010) faces rather than on the (001) one, therefore suggesting an easier growth along the *c*-direction of hydroxyapatite crystals from AA solutions.

Submitted to Philosophical Transactions A for the themed issue "Structure and Activity of Bioceramics".

Introduction

The study of the biomolecule/biomaterial interactions is an actual gaining-ground research field because of the potentiality of nanotechnology applied to biotechnological processes and in biomedical applications [1-5]. Among various biomaterials, hydroxyapatite [HA, $Ca_{10}(PO_4)_6(OH)_2$] is the natural major inorganic constituent of bone and teeth and thus often used as a reference to study biomolecule/biocompatible-surface interactions [6,7]. Among biomolecules, proteins are by far the most interesting, due to their adhesion to HA surfaces. This is particularly the case for bone tissue regenerators, since protein adhesion to implants and prostheses is crucially mediated by processes occurring at their surfaces. Indeed, functionalizing HA-based materials - as for the case of the bioglass surfaces - to enhance their biocompatibility is a common target [8,9]. Furthermore, understanding the protein/HA contact is of relevance in biomineralization processes[10] since HA grows spontaneously outside the Hench 45S5® Bioglass (45% SiO_2 – 24.5% Na_2O – 24.5% CaO – 6% P_2O_5), when the latter is contacted with simulated body fluids (SBF) [11]. In that respect, the HA growth rate is well-known to be strongly influenced by the biological composition of the SBF, *i.e.* different amino acids, peptides and proteins may inhibit the HA growth to a different degree. Additionally, calcium phosphate-based nanoparticles have been proposed as suitable materials for loading and securing different drugs, to be delivered afterwards in a controlled way inside a living body [12,13].

The ultimate goals when studying protein/HA-surface interactions are: i) to know how the AA side-chains interact with the HA surfaces and ii) based on point i), to understand how proteins change their native conformation as a result of the adsorption process. As for point i), adsorption isothermal experiments as well as conventional high-resolution spectroscopy studies have been performed to determine both macroscopic quantities and the actual interaction interface of statherin [14-20], myoglobin [21,22], amelogenin [23,24], bovine serum albumin [24-26], bovine serum fibrinogen [26], lysozome[25,26] and proline-rich protein PRP1[27] upon HA adsorption. Most of these papers conclude that proteins are generally adsorbed by electrostatic forces of different strength depending on the protein structure and AA sequence. It is worth mentioning that merging several of the mentioned techniques has allowed to identify the statherin amino acidic residues involved in the interaction with HA, as is beautifully reviewed in reference [19]. As for point ii), it is usually observed

that proteins denature due to contact with inorganic solid substrates. However, recent findings highlight HA surfaces as ideal platforms to stabilize (and even to induce) well-defined protein folded conformations upon adsorption [17,28], a fact which enables the retention of the peptide biological functionality.

Despite the wide experimental investigations dedicated to protein/HA systems, detailed atomistic features related to the binding mechanisms and the anchoring points occurring at HA surfaces remain relatively scarce. To this respect, several classical molecular dynamics-based studies are present in the literature [29-31], focusing on the dynamic behavior of proteins in water and when driven to the surfaces. The adoption of classical force fields (FF) needed to handle the large number of atoms involved, inevitably lower the accuracy of the results, as actual FF cannot cope with bond breaking/making which may indeed occur between side-chain functionalities and the HA surface. Resorting to quantum mechanical methods ideally solves this problem: however, modeling protein/HA interaction at this level remains almost impossible. Nevertheless, by following a hierarchical approach, the interaction with single AA allows to learn how side-chains interact with the HA surface. The outcome of this approach is twofold: i) to understand the influence of AA on the HA surfaces growth, as recent experiments have addressed [32-35]; ii) to provide accurate benchmark data for the development of specific FF devoted to simulate protein/HA interactions. We have recently published ab-initio results for the gas-phase adsorption of glycine (Gly), at (001) and (010) HA surfaces, providing a detailed molecular picture of the Gly/HA interface in absence of water [36]. The present paper extends that study by reporting the interaction (structure and energetics) of polar non-aromatic AA (serine Ser, lysine Lys, glutamine Gln and glutamic acid Glu) on HA surfaces by means of periodic B3LYP calculations. The simulation of the AA interaction onto HA surfaces in complete dried conditions is particularly interesting because it allows understanding the intrinsic AA/HA features, free from the influence of water, although it was recently shown by some of us that the Gly/HA adducts with the presence of some water molecules are very similar to the free-water ones, since Gly interacts directly towards the surface and water behaving as spectator [37]. It is worth noting that, indeed, a number of AA may be easily sublimated [38] and their spectral features in gas-phase have been studied at very high resolution [39,40]. This feature has been used to adsorb Gly by chemical vapor deposition on amorphous silica[41] and by some of us on HA nano-crystals [42]. In both cases only the combination with quantum mechanical results allowed to resolve the

atomistic and vibrational details of Gly on both surfaces at an unprecedented level of details. In the present work we only focused on the structural and energetic features as the vibrational analysis would have been rather cumbersome to describe without the experimental counterpart to compare with, which is, to our knowledge, still missing.

Computational Details

In the following only essential computational details are provided leaving full account to the SI. All the periodic calculations of the interaction of the considered AA with the HA (001) and (010) faces have been performed with the ab-initio code CRYSTAL06 [43] using a Gaussian basis set of polarized double-zeta quality already adopted in previous studies [44]. All the SCF calculations and geometry optimizations were performed with B3LYP density functional method [45,46] using 10 reciprocal *k*-points to sample the Brillouin zone. Geometries were optimized by relaxing the internal coordinates within *P1* symmetry keeping the lattice parameters fixed at the values of the optimized bare surfaces.

In a periodic treatment, the adsorption energy ΔE per unit cell per adsorbate is defined as:

$$\Delta E = E(\mathrm{SM//SM}) - E(\mathrm{S//S}) - E_m(\mathrm{M//M})$$

where E(S//S) is the energy of the bare HA slab S in its optimized geometry, E_m(M//M) is the molecular energy of the free amino acid molecule M in its optimized geometry and E(SM//SM) is the energy of the considered HA/AA system in its optimized geometry (the symbol following the double slash identifies the geometry at which the energy has been computed). ΔE is a negative quantity for a bound system and can be recast in terms of deformation cost of the surface δE_S, the adsorbate ΔE_M, the lateral adsorbate-adsorbate interactions ΔE_L, and the interaction ΔE^* between the pre-deformed constituents. The final expression ΔE^C, inclusive of the BSSE correction reads:

$$\Delta E^C = \Delta E + \mathrm{BSSE} = \Delta E^{*C} + \delta E_S + \Delta E_M + \Delta E_L \; ; \quad \mathrm{BSSE} = \Delta E^{*C} - \Delta E^*$$

Because B3LYP did not include dispersion energy, the post-DFT dispersive correction suggested by Grimme [47] and re-parameterized by some of us for periodic systems (referred as D*) [48], has been added to the BSSE-corrected adsorption energies ΔE^C in a posteriori fashion to obtain the final $\Delta E^C + D^*$. In this way the

dispersive contribution is inserted in a non-self-consistent way to the adsorption energy, which, somehow, underestimates its relevance.

Results and Discussion

This section is organized as follows: i) a brief description of the structural features for the (001), (010) and (010)w stoichiometric HA surfaces; ii) the most relevant structural information derived from the interaction of each AA on the three HA surfaces; iii) the adsorption energy values of the AA/HA systems; iv) a comparison of the affinity of different AA for each surface.

HA surface models

For the sake of brevity, here we only report the most relevant structural and energetic features of the stoichiometric (001) and (010) HA surfaces, as further details have been already reported in recent papers [49-51]. The HA (001) and (010) surfaces are the most relevant from a biological point of view: the (001) plane is the dominant surface in the thermodynamic morphology [52-54], whereas the crystal growth occurs overall through the *c*- direction during biomineralization, thereby the (010) face resulting very extended in the final HA crystal and often responsible for interaction with molecules [55-57]. These two surfaces were modeled within the slab approach by selective cuts of the optimized bulk structure. They are both perfect planes, without defects (vacancies, steps or kink sites), and their thicknesses are 14 Å for the (001) case (fully optimized within the *P3* layer group) and 13 Å for the (010) case (*P1* symmetry). The geometry optimizations for AA adsorption were carried out within the *P1* symmetry for both cases. To simulate the effect of both low and high AA surface coverage, two unit cells were adopted (see Figure 1): the single-cell, consistent with the unit cell of HA bulk and a double-cell, derived from the single cell by doubling the *a* and the *c* values for the (001) and the (010) surfaces, respectively.

The (001) surface unit cell exhibits two Ca ion types (Ca1 and Ca3), whereas for the (010) surface three Ca types (Ca1, Ca2 and Ca3) exist (see Figure 1a and 1b, respectively). The analysis of the electrostatic potential features (not shown) reveals high positive values of potential on top of Ca ions (suggesting compatible sites for AA electron donor groups), whereas deep negative zones are located in the proximity of oxygen atoms of the PO_4 groups (suggesting H-bond interactions with AA H-bond donor groups).

The (001) slab exhibits a smaller surface energy than the (010) one (1.043 and 1.709 J m^{-2}, respectively, at B3LYP level) [50,51] because the number and type of bonds that should be cut to define the (010) surface impart a higher cost in comparison with the (001) surface. Therefore, the (010) model is expected to be more reactive. This was indeed the case for water adsorption, which is molecularly adsorbed at the (001) surface whereas spontaneously dissociates on the Ca1 and Ca2 sites of the (010) surface while is molecularly adsorbed on Ca3 ion [51,58]. Owing to this fast reaction with water (ubiquitously present during crystal growth), the pristine HA (010) surface is unlikely to exist "as cut" from the HA bulk, therefore the AA adsorption at the water-reacted HA (010) surface (hereafter named as (010)w surface) was also considered in this work. The most stable reconstructed (010)w surface is shown in Figure 1c, in which the H_w and OH_w label the new functionalities resulting from water dissociation and giving rise to POH and CaOH groups, respectively. The newly formed OH_w group is shared by Ca3, Ca2a and Ca2b ions with a local geometry resembling that surrounding the OH group of the HA (001) surface (Figure 1). It is clear that this particular geometrical arrangement gives stability to the final structure and it is worth noting that H_2O does not dissociate on Ca1 (*vide supra*) because the surface OH cannot be similarly stabilized. The reactivity of the pristine (010) and the (010)w surfaces can be appreciated by considering the energy of adsorption with respect to H_2O computed at B3LYP level with the same basis set adopted here [51]: -315 and -249 kJ/mol for H_2O *chemisorbed* on Ca3 and Ca2 ions of the (010) surface, respectively to be compared with the much lower value of -92 kJ/mol for H_2O *physisorbed* on Ca1 of the (010)w surface. It is then expected that a similar difference in reactivity will be shown for the AA adsorption (*vide infra*).

Strategies for AA adsorption

AA were manually docked to the HA surfaces in agreement with the electrostatic complementarity between the two partners and the resulting adducts used as initial structures for the full B3LYP optimization. In the present study, the AA were adsorbed only at the top face of the slabs. This yields a permanent dipole perpendicular to the surface due to the asymmetry introduced between the two surfaces (top/bottom), which may affect the adsorption energy values. We check the dependency of the adsorption energy of Gly when adsorbed at the (001), (010) and (010)w HA surfaces for top and top/bottom cases. Results are available in the SI (Figure S1 and Table S1) and

show differences in the adsorption energy between top and top/bottom cases of 7 kJ mol^{-1} at the most, which is very small considering the large computed values (around -250/-450 kJ mol^{-1}). This allowed simulating the AA adsorption at the top face only, with a significant saving in computer time.

The glycine/HA surface systems

As reported in previous simulations [36,59], Gly adsorbs as a zwitterion on the (001) surface (**001-Gly,** Figure 2). The stabilization is due to the simultaneous presence of COO^-/Ca^+ electrostatic interactions and H-bonds between NH_3^+ protons and surface oxygen atoms of the PO_4 group. This structure is the most stable in both single- and double-cell slab models. It is worth noting that, contrary to the metal ion $[Ca\text{-}Gly]^{2+}$ complex occurring in gas phase [60], with only one Ca ion as coordinator center, in **001-Gly** two different Ca ions are simultaneously involved in the Gly adsorption, resulting in a larger stabilization due to the enhanced electrostatic interactions.

At the (010) surface Gly interacts through a Gly^-/HA^+ ion pair (**010-Gly**, Figure 2) as the proton is transferred to the surface (occurring from COOH or NH_3^+ for neutral and zwitterion forms, respectively), in agreement with previous works [36,59]. The remaining COO^- group interacts with three Ca ions. In particular, the O1 of the COO^- group is shared, almost equivalently, with Ca2a (Ca2a-O1: 2.584 Å), Ca2b (Ca2b-O1: 2.426 Å) and Ca3 (Ca3-O1: 2.411 Å) ions; the second oxygen O2 of the COO^- group interacts more strongly with Ca2a (Ca2a-O2: 2.349 Å, Figure 2) while the NH_2 acts as H-bond acceptor from the POH surface groups formed by the protonation process (H···N: 1.611 Å).

The proton transfer towards the HA surface also occurred on the water reacted HA (010)w surface (**010w-Gly**, Figure 2), the basic PO_4 surface group becoming protonated. Because at the pristine (010)w surface the Ca2a, Ca2b and Ca3 ions (those anchoring Gly in **010-Gly**) are already engaged in the interaction with the OH_w resulting from the dissociated H_2O (*vide supra*), the COO^- group interacts with the remaining Ca1 (Ca1-O2: 2.384 Å), Ca2a (Ca2a-O1: 2.566 Å) and Ca2b (Ca2b-O1: 2.435 Å) ions. The NH_2 group interacts with the newly created POH functionality (derived from the Gly deprotonation) by a rather strong H-bond (H…N: 1.683 Å). A comparison of the adsorption energies between the **010-Gly** and **010w-Gly** adducts (see Table 2) reveals that Gly is adsorbed stronger on the pristine surface than on the water reacted one, as anticipated (*vide supra*). This is due to: i) a higher reactivity of the Ca2a,

Ca2b and Ca3 ions of the (010) surface compared to the Ca1, Ca2a and Ca2b ions of the water reacted (010)w one; ii) the decreased basic character of the PO_4 groups on the (010)w surface in comparison to the (010) one.

The features of the Gly/HA structures are then adopted as a reference for the other AA, as the common $COOH/NH_2$ moiety was assumed to behave similarly to what is found for Gly, while the side chains specifically interact with the remaining surface functionalities. For that, the common features to all AA will no longer be discussed.

Structure of the polar AA/HA surface systems

The B3LYP-optimized geometries of Ser, Lys, Gln and Glu interacting with the HA surfaces are illustrated in Figures 3, 4, 5 and 6, respectively. Table 1 reports the most relevant structural features.

Serine. Ser (exhibiting a CH_2OH side chain functionality) adsorbs on the (001) surface forming a H-bond between the surface PO_4 and the OH groups (**001-Ser**, Figure 3) for both single- and double-cell slab models. The optimized structure also exhibits an electrostatic interaction between a Ca ion and the side chain oxygen atom (Ca3b-O3), although it is weaker (Ca3b-O3 distance of 2.5 Å) compared to that involving the backbone Ca-COO moiety (around 2.3 Å).

Ser interacts with the (010) surface via an additional H-bond and the Ca2b-O3 bond (**010-Ser**, Figure 3), this latter missed with the (010)w surface (**010w-Ser**, Figure 3) due to the engagement of the Ca ions by the pristine OH_w.

Lysine. Lys (with a $(CH_2)_4NH_2$ side chain functionality) adsorbs on the (001) surface via the N atom through the Ca1 ion, without forming any H-bond interactions (**001-Lys**, Figure 4). This occurs in both the single and the double cell models, the Ca1-N bond distance being moderately different. In the single-cell slab model (simulating high Lys loading), the Ca1 already engaged with the O1 backbone carboxylate atom also interacts with the N side chain atom of an image Lys of the adjacent unit cell, giving rise to Lys-Lys repulsive lateral interaction. This is illustrated in Figure 4, where the terminal NH_2 groups of the image Lys molecule is depicted in sticks. In contrast, in the double-cell slab model (simulating low Lys loading) two independent Ca1 ions exist, so that one interacts with O1 and the other with the N side chain atom (picture not reported). Accordingly, for the single-cell slab, the Ca1-O1 and Ca1-N bond distances are longer than for the double one by about 0.010 Å.

With the (010) HA surface the interactions, in both slab models, are through the N side chain atom and the free Ca1 ion (**010-Lys**, Figure 3). For the single-cell (010)w slab, the NH_2 side chain H-bonds with the POH_w surface and also with the image Lys (**010w-Lys**, Figure 4). For the double-cell (010)w slab, the side chain N atom binds to the free Ca2a ion (see **010w-Lys(dc)** of Figure 4), as it will occur for Gln and Glu cases (*vide infra*).

Glutamine and Glutamic acid. The features of the Gln and Glu adsorbates are similar, despite the differences in their side chain functionalities ($(CH_2)_2CONH_2$ and $(CH_2)_2COOH$, respectively). For both amino acids the C=O side chain groups interact with Ca1 (Ca1-O3 bond), whereas the side chain protons (NH and OH for Gln and Glu, respectively) H-bond with the PO_4 surface groups (**001-Gln** and **001-Glu**, Figure 5 and 6, respectively). The H-bond established by the Glu side chain is notably stronger than the one established by the Gln side chain (1.4 *vs* 1.7 Å, respectively) because of the stronger acidic character of the COOH group.

Similar facts are observed for the adsorption of Gln and Glu on the (010) surface, modeled by means of a single-cell slab (**010-Gln**, **010-Glu**, **010w-Gln**, **010w-Glu** of Figure 5 and 6, respectively). Nonetheless, significant changes are observed with a double-cell slab model: i) at the (010) surface, the Ca2a-O3 bonds become stronger (with a shortening of about 0.5 and 0.2 Å, for Gln and Glu, respectively, see Table 1); ii) the H-bonds (values *c* in Figure 5 and 6 and Table 1) between AA images disappear with the double-cell; iii) at the (010)w surface, the Glu and Gln C=O side chain groups interact with the Ca2a atom (see **010-Gln(dc)** and **010-Glu(dc)** of Figure 5 and 6, respectively). An additional H-bond is established (H-bond labeled as *c* in Figure 5), in which, for the particular case of Glu, the acidic proton was transferred to a PO_4 surface group.

Adsorption energies for all considered models.

Values of the adsorption energy, non-corrected (ΔE), BSSE-corrected (ΔE^C), and including dispersive forces (ΔE^C+D*) are reported in Table 2, whereas Figure 7 depicts the AA affinity ladders towards the HA surfaces and Figure 8 the relative increment in the interaction energies with respect to Gly, assumed as a reference (*vide infra*). For periodic systems the BSSE can only be evaluated for cases in which both the adsorbate and the surface remains electroneutral so that are excluded all processes in which bond making/breaking occur. Only adsorption at the (001) surface brings about neutral

constituents and the BSSE resulted about 45–49% of the interaction energies. For the other surfaces we simply assumed a fixed 45% BSSE resulting from averaging over the BSSE% for the (001) cases and the resulting BSSE corrected interaction energies are labelled $\Delta E^{C\text{-}est}$ in Table 2. A different possibility is to assume a fixed BSSE for each AA, also derived from the analysis of the interaction energies for the (001) case and to correct all cases from the (010) and (010)w surfaces. This approach will change the absolute values of $\Delta E^{C}+D^{*}$ compared to the previous strategy (in particular for the (010) case) but will essentially preserve the relative trend (see Figure S3 of the supplementary information). Nevertheless, this different approach brings some inconsistency in the data, as the $\Delta E^{C}+D^{*}$ data for Ser on the (010)w surface resulted less negative (smaller binding energy) than for Gly, a behavior difficult to understand owing to the OH group involved in a rather strong H-bond with the (010)w surface for Ser, which is missing in Gly.

HA (001) surface. The affinity of the AA for the HA(001) surface monitored by the ($\Delta E^{C}+D^{*}$) adsorption energies (reported in Table 2) shows the Gly < Ser < Lys ≈ Gln < Glu trend (see Figure 7). The $\Delta E^{C}+D^{*}$ values are higher (in absolute term) compared to those for other molecules (~-100 kJ mol^{-1} for water,[51,58] or ~-80 kJ mol^{-1} for citric acid[61]) and of the same order for proline and hydroxyproline (~-300 and ~-500, respectively) [59], showing that polar amino acid side-chains interact strongly with HA surfaces. The dependency of the interaction energy as a function of the cell size is rather limited (see Table 1 and Figure 7). The largest differences are shown by the ΔE^{C} values, but they become less important due to the subtle interplay of the dispersive contribution, which is larger for the single-cell model due to the favorable lateral interactions.

The ΔE energy contributions (available in SI, Table S2) show that the highest surface energy deformation δE_S values occur for AA with the largest number of surface specific interactions, which, in turn, increases energy deformation cost ΔE_M of the adsorbate.

HA (010) and (010)w surfaces. The affinity of the AA for the HA(010) and (010)w surfaces monitored by the ($\Delta E^{C\text{-}est}+D^{*}$) adsorption energies (reported in Table 2 and in Figure 7) show: i) for HA (010), the Gly < Ser < Lys < Gln < Glu (single-cell)

and Gly < Ser < Gln < Lys < Glu (double-cell) trends; ii) for HA (010)w, the Gly < Ser < Glu < Gln <Lys (single-cell) and Gly < Ser < Glu ≈ Gln < Lys (double-cell) trends. The differences are essentially connected to the positions between Lys, Gln and Glu, so it seems that their strength of adsorption is a delicate balance between the intrinsic affinity of the AA towards HA (modulated by electrostatic, H-bond and dispersive interactions) as well as the surface morphology (pristine or water reacted (010) surface) and the amount of AA already adsorbed. Despite that, results clearly indicate that Gly and Ser exhibit the lowest adsorption energies, whereas Lys, Gln and Glu the largest ones.

Additional notes on adsorption energies. In order to have a deeper insight into the driving forces for AA adsorption we computed the interaction energies of the same AA with a free Ca^{2+} ion, forming the doubly-charged $[Ca\text{-}AA]^{2+}$ ion complex. It is well-known that the most stable gas-phase $[Ca\text{-}Gly]^{2+}$ isomer exhibits Gly in its zwitterionic state [60]; however, structural information on the remaining $[Ca\text{-}AA]^{2+}$ ion complexes is scarce. Thus, we simulated the $[Ca\text{-}AA]^{2+}$ ion complexes, in which the amino acids are both in their neutral and zwitterionic state. For both cases we computed the interaction energy in order to obtain a consistent electrostatic trend of the lateral chains in interaction with Ca ions. Structures and energies of the computed $[Ca\text{-}AA]^{2+}$ ion complex are available in SI (Figure S2 and Table S3). For both AA forms, the obtained trends follow Gly < Ser < Glu ≈ Gln < Lys, which is in agreement with the Lewis basic character of the lateral chains (OH < CO < NH_2). This scale is somehow similar to those obtained for the AA adsorption onto HA surfaces, the main differences arising from the positions of Lys, Gln and Glu. Therefore, it seems that, on one hand, the possible H-bonds between Gln and Glu with the surfaces and, on the other, the large dispersive interactions between Lys and the surfaces alter the magnitude of interaction, giving rise to the different scale affinities reported above.

All AA have in common with Gly the $NH_3^+CHCOO^-$ moiety which exhibits the same interactions with the HA surfaces for all considered AA. Because of that, it is possible to compute the excess of interaction energy of a given AA with respect to Gly, as due to the specific affinity of its side chain for the HA surfaces. This quantity, named $\Delta T=[\Delta E^C+D^*]_{Gly} - [\Delta E^C+D^*]_{AA}$ is shown in Figure 8 (leftmost column) for both single and double cell models. Because $[\Delta E^C+D^*]_{Gly}$ is less negative than $[\Delta E^C+D^*]_{AA}$

for all AA, their difference is always a positive quantity. The pure dispersion contribution to ΔT is also shown as $\Delta D^* = D^*_{Gly} - D^*_{AA}$ in the same figure (rightmost column) and again is always a positive quantity. The single cell model (SC) represents a high loading of AA at the HA surfaces and it turns out that: i) the smallest increment is due to CH_2OH (Ser) side chain for all surfaces; ii) the ΔT is almost constant at 75 kJ mol^{-1} for the (001) surface for all AA but for Ser; iii) at the (010) the ΔT increases monotonically along the Ser > Lys > Gln > Glu series, whereas for the (010)w the behavior is dramatically different, Lys being the highest and Ser and Glu showing almost the same value. The dispersion contribution ΔD* to ΔT is totally dominant for Gln and Glu on the (010)w showing that the specific interactions with the lateral chains are inhibited for these AA, whereas it amounts about a half of ΔT for all other cases and surfaces. The double cell case (DC) mimics a low AA loading. For the (001) surface, the ΔT trend is similar to SC, with ΔT values being all slightly higher. For the (010) surface the three Lys, Gln and Glu exhibit a very similar ΔT value at variance with the SC case. The most dramatic changes is for the (010)w surface which shows higher ΔT increments compared to the SC as now the side chain groups can exploit the surface functionalities in a more efficient way. The ΔD* values are similar to those of the SC case, with Lys having the highest contributions for the (010) and (010)w surfaces.

It is worth to analyze the computed adsorption energies as a function of the surface type and of the kind of AA. Results indicate that the pristine (010) surface is more reactive than the hydrated (010)w surface which, in turn, exhibits more favourable adsorption energies than the (001) one. This fact allows to understand the growth and the final surface morphology of the HA crystals in presence of physiological fluids. That is, by extending our results to biological systems, proteins would prefer to adsorb at the (010) face so that the growth rate along its direction would be inhibited, in favor of the growth along other directions. Additionally, the fact that the computed adsorption energies are so favorable suggests that proteins containing the tested amino acidic residues, specially carrying Ca binding or H-bond donor groups, will serve as inhibitors of the HA growth. In particular our results estimate that C=O and NH_2-containing lateral chains of proteins may be of use to control the growth of calcium phosphate materials.

Conclusions

The adsorption of 5 AA with different physic-chemical properties (Gly as non-polar, Ser as polar/neutral, Lys as polar/basic, Gln as polar/amidic and Glu as polar/acidic) on models of stoichiometric (001), (010) and (010)w HA surfaces under strict gas-phase conditions has been studied with B3LYP and Gaussian type basis set in a periodic approach using the CRYSTAL06 code. AA were manually docked towards the HA surface following the electrostatic complementarity and by maximizing H-bond interactions. High and low AA loadings have been simulated by adopting two unit cell sizes. The most interesting points emerged from the present work are summarized as follows:

i) Gly is adsorbed as a zwitterion at the HA (001) surface, the COO^- group interacting with two Ca ions and the NH_3^+ protons H-bonding the oxygen surface atoms, whereas on both the pristine (010) surface and the reacted with water (010)w, a Gly^-/HA^+ ion pair is established;

ii) For the other AA, the adsorption occurs keeping the common $NH_3^+CHCOO^-$ moiety in the same configuration as for Gly, while leaving the side chain groups to maximize the interaction with the available surface sites;

iii) For Gly and Ser no significant differences are observed between SC and DC models, whereas the adsorption for Lys, Gln and Glu is much more sensitive to lateral interactions. For these latter a general increase in the strength of interaction is computed when moving from SC to DC;

iv) The driving forces for AA adsorption are the electrostatic affinity for Ca ions, H-bonds towards the basic PO_4 surface groups and the dispersive interactions. When the contribution of the common $NH_3^+CHCOO^-$ moiety is subtracted from the interaction energy (ΔT values) it emerges that the AA affinity averaged over all HA surfaces, for the low AA loading (DC case) follows the trend: CH_2OH(Ser 35 $kJmol^{-1}$) < $(CH_2)_2CONH_2$(Gln 81 $kJmol^{-1}$) < $(CH_2)_2COOH$(Glu 91 $kJmol^{-1}$) ≈ $(CH_2)_4NH_2$(Lys 92 $kJmol^{-1}$). Clearly, Lys is able to sample the Ca ions with the greatest affinity and the long hydrocarbon chain gains dispersion energy. These incremental values can constitute a database for predicting the proteins affinity towards HA by the knowledge of the exposed side chains.

v) For all cases, the interaction with the (010) faces were found to be more favorable than the (001) one, indicating a major reactivity of the former surfaces. According to these results, protein amino acidic residues prefer to adsorb on the (010) faces, thereby inhibiting more strongly the crystal growth of these surfaces and consequently leading to an elongated morphology in the *c*-direction of the apatite crystal.

vi) Purely geometrically defined surfaces may not be representative of the corresponding surface in the real material, as reaction with water may deeply alter the adsorption character of the pristine surface. Here, the water reacted (010)w surface exhibits much weaker adsorption energies with respect to those computed for the pristine (010) surface.

Results of the present paper are aimed at contributing with significant clues on the structure and energetics that drives the protein/calcium-apatites interactions, such as to provide a detailed atomistic picture of the interface between AA and HA, or to estimate an affinity scale for the interaction of polar amino acidic residues with HA surfaces. Along this line, it is worth mentioning that such free-water systems are indeed possible to study by means of IR spectroscopy due to the development of the fast thermal heating technique [39,40], which allows experimentalists to adsorb neutral AA on HA by chemical vapor deposition. In that respect, new experimental measurements under highly controllable conditions would be welcome and could be used for direct comparisons and to validate the present results.

Acknowledgement

A.R. is indebted to "Comissionat per a Universitats I Recerca del Deprtament D'Innovació, Universitats I Empresa de la Generalitat de Catalunya". Financial support from MIUR (Project COFIN2006, Prot. 2006032335_005), from the Regione Piemonte (Bando ricerca scientifica Piemonte 2004, Settore: Nanotecnologie e nanoscienze, "Materiali nanostrutturati biocompatibili per applicazioni biomediche"), and from MICINN through the CTQ2008-06381/BQU project is gratefully acknowledged. P.U. kindly acknowledges BSC-MN for the generous allowance of computing time through the "BCV-2008-2-0013: Simulation of peptide folding induced by inorganic materials" and "BCV-2008-3-0013: Simulation of peptide folding induced by inorganic materials II" projects.

Table 1. B3LYP-optimized bond lengths of the different amino acids/HA structures. Bare values belong to single-cell systems, in brackets to the double-cell ones. Units in Å.

	HA(001)							
structure	Ca1-O1	Ca3c-O2	Ca3b-O3	Ca1-N	Ca1-O3	*a*	*b*	*c*
001-Gly	2.334 (2.330)	2.354 (2.366)				1.622 (1.618)	1.956 (1.945)	
001-Ser	2.372 (2.339)	2.375 (2.379)	2.582 (2.599)			1.709 (1.695)	1.875 (1.897)	1.507 (1.485)
001-Lys	2.405 (2.396)	2.334 (2.346)		2.443 (2.436)		1.705 (1.676)	1.760 (1.799)	
001-Gln	2.369 (2.348)	2.378 (2.360)			2.444 (2.380)	1.629 (1.665)	2.011 (1.843)	1.727 (1.754)
001-Glu	2.359 (2.334)	2.362 (2.358)			2.427 (2.401)	1.662 (1.669)	2.093 (1.922)	1.450 (1.379)

	HA(010)									
structure	Ca3-O1	Ca2a-O1	Ca2b-O1	Ca2a-O2	Ca2b-O3	Ca1-N	Ca2a-O3	*a*	*b*	*c*
010-Gly	2.411	2.584	2.426	2.349				1.611	1.857	
	(2.408)	(2.542)	(2.380)	(2.349)				(1.501)	(1.838)	
010-Ser	2.392	2.523	2.406	2.410	2.488			1.620	2.086	1.635
	(2.390)	(2.476)	(2.381)	(2.383)	(2.500)			(1.562)	(2.103)	(1.663)
010-Lys	2.445	2.589	2.472	2.393		2.633		1.617	2.071	
	(2.429)	(2.531)	(2.407)	(2.356)		(2.679)		(1.532)	(2.030)	
010-Gln	2.406	2.835	2.446	2.376	2.374		2.988	1.627	1.989	1.662
	(2.435)	(2.566)	(2.416)	(2.410)	(2.436)		(2.484)	(1.539)	(2.086)	(-)
010-Glu	2.428	2.826	2.463	2.395	2.395		2.850	1.610	2.012	1.487
	(2.435)	(2.563)	(2.399)	(2.374)	(2.462)		(2.669)	(1.535)	(2.183)	(-)

	HA(010)w					
structure	Ca1-O2	Ca2a-O1	Ca2b-O1	*a*	*b*	*c*
010w-Gly	2.384 (2.385)	2.566 (2.498)	2.435 (2.410)	1.683 (1.667)	2.127 (2.073)	
010w-Ser	2.301 (2.278)	2.469 (2.402)	2.498 (2.508)	1.827 (1.806)	2.115 (2.303)	1.702 (1.706)
010w-Lys	2.342 (2.315)	2.415 (2.521)	2.444 (2.466)	1.983 (1.706)	1.577 (1.952)	2.071 (-)
		Ca2a-N (2.559)*				
010w-Gln	2.302 (2.328)	2.528 (2.527)	2.455 (2.450)	1.881 (1.762)	1.733 (1.931)	- (2.009)
		Ca2a-O3 (2.357)*				
010w-Glu	2.288 (2.329)	2.571 (2.522)	2.417 (2.442)	1.892 (1.748)	2.105 (1.934)	- (1.834)
		Ca2a-O3 (2.368)*				

*See structures 010w-Lys(dc), 010w-Gln(dc) and 010w-Glu(dc) of Figure 4, 5 and 6, respectively.

Table 2. Computed adsorption energies for the different amino acids/HA systems with single-cell and double-cell slab models: non-corrected (ΔE) and BSSE-corrected (ΔE^{C}) adsorption energies; estimated ΔE^{C} values considering the percentage of the BSSE upon ΔE of 45% ($\Delta E^{C\text{-}est}$, see text for details), contribution of the dispersive forces (D^*) by single-point energy evaluation on the B3LYP optimum structures and ΔE^{C} and $\Delta E^{C\text{-}est}$ including the term D^* ($\Delta E^{C}+D^*$ and $\Delta E^{C\text{-}est}+D^*$, respectively). Units in kJ mol^{-1}.

system	single-cell				double-cell			
	$-\Delta E$	$-\Delta E^{C}$	$-D^*$	$-(\Delta E^{C}+D^*)$	$-\Delta E$	$-\Delta E^{C}$	$-D^*$	$-(\Delta E^{C}+D^*)$
001-Gly	248	136	54	190	251	141	43	184
001-Ser	312	160	77	237	316	168	65	233
001-Lys	324	173	86	259	347	191	71	262
001-Gln	329	168	94	262	343	180	76	255
001-Glu	342	179	90	269	368	203	75	278
010-Gly	449	247	70	317	449	245	68	313
010-Ser	484	266	79	345	491	270	85	355
010-Lys	528	290	99	389	534	293	126	419
010-Gln	543	299	105	404	555	305	110	415
010-Glu	571	314	120	434	579	318	107	425
010w-Gly	323	178	63	240	318	175	57	232
010w-Ser	329	181	77	258	324	178	68	245
010w-Lys	373	205	102	307	371	204	115	324
010w-Gln	328	181	96	277	372	205	98	302
010w-Glu	314	172	91	263	380	209	95	300

Figure Captions

Figure 1. B3LYP-optimized geometries of the double-cell hydroxyapatite (HA) surfaces used in the present work. Single-cell slab models defined as grayed regions.

Figure 2. B3LYP-optimized geometries of Gly with the considered HA surfaces. Geometry parameters are reported in Table 1.

Figure 3. B3LYP-optimized geometries of Ser with the considered HA surfaces. Geometry parameters are reported in Table 1.

Figure 4. B3LYP-optimized geometries of Lys with the considered HA surfaces. The (dc) label identifies the double-cell slab model. Geometry parameters are reported in Table 1.

Figure 5. B3LYP-optimized geometries of Gln with the considered HA surfaces. The (dc) label identifies the double-cell slab model. Geometry parameters are reported in Table 1.

Figure 6. B3LYP-optimized geometries of Glu with the considered HA surfaces. The (dc) label identifies the double-cell slab model. Geometry parameters are reported in Table 1.

Figure 7. AA affinity ladders towards the HA surfaces according to the computed adsorption energies $\Delta E^{C}+D^{*}$. Solid lines refers to single-cell slab models, dashed lines to double-cell ones.

Figure 8. Top: $\Delta T=[\Delta E^{C}+D^{*}]_{Gly}$ - $[\Delta E^{C}+D^{*}]_{AA}$ and $\Delta D^{*}=D^{*}_{Gly}$ - D^{*}_{AA} for single-cell (SC) and double-cell (DC) slab models.

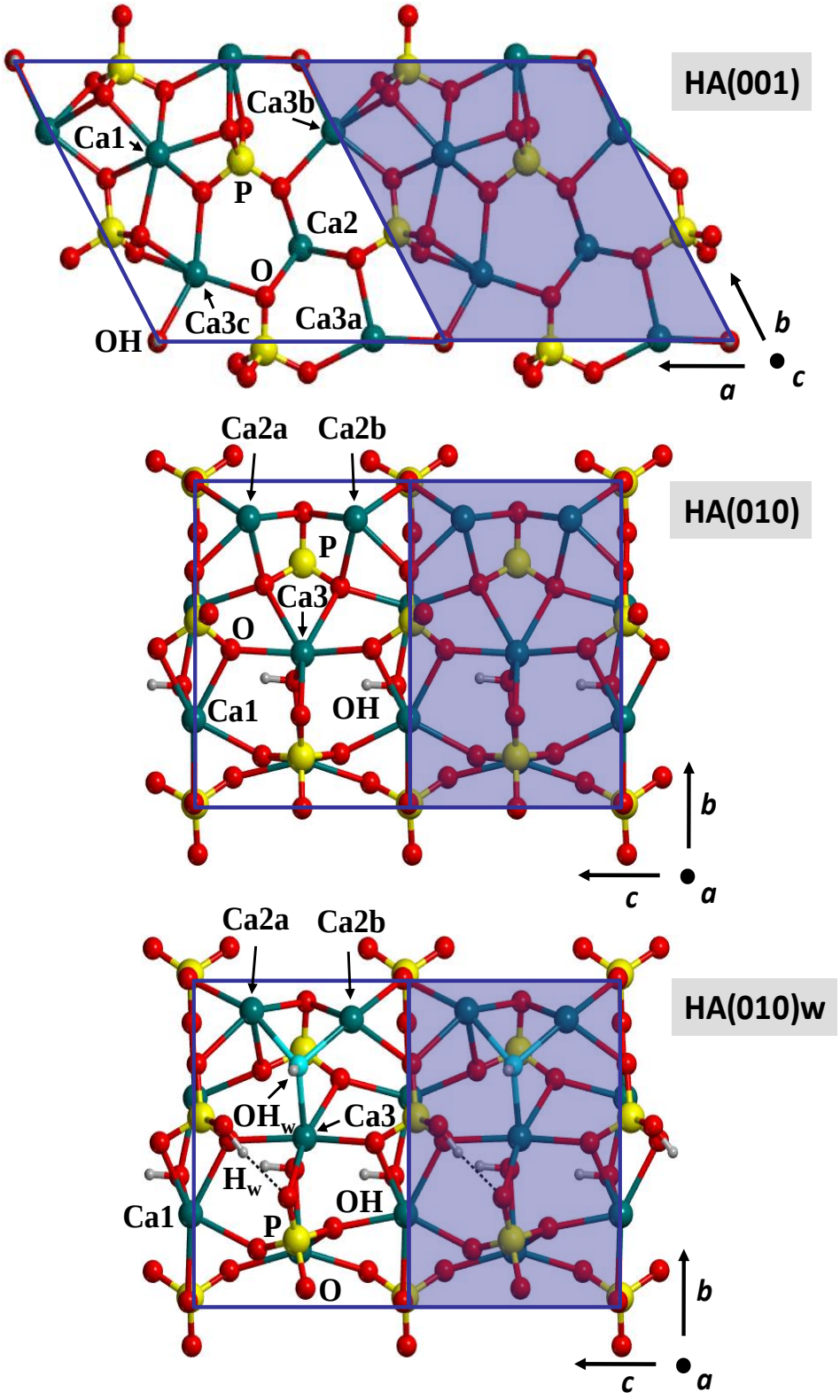
HA(001)
Ca3b
Ca1
P
Ca2
O
Ca3c
Ca3a
OH
b
c
a
Ca2a
Ca2b
HA(010)
P
Ca3
O
Ca1
OH
b
c
a
Ca2a
Ca2b
HA(010)w
OHw
Ca3
Hw
OH
Ca1
P
O
b
c
a

Figure 1.

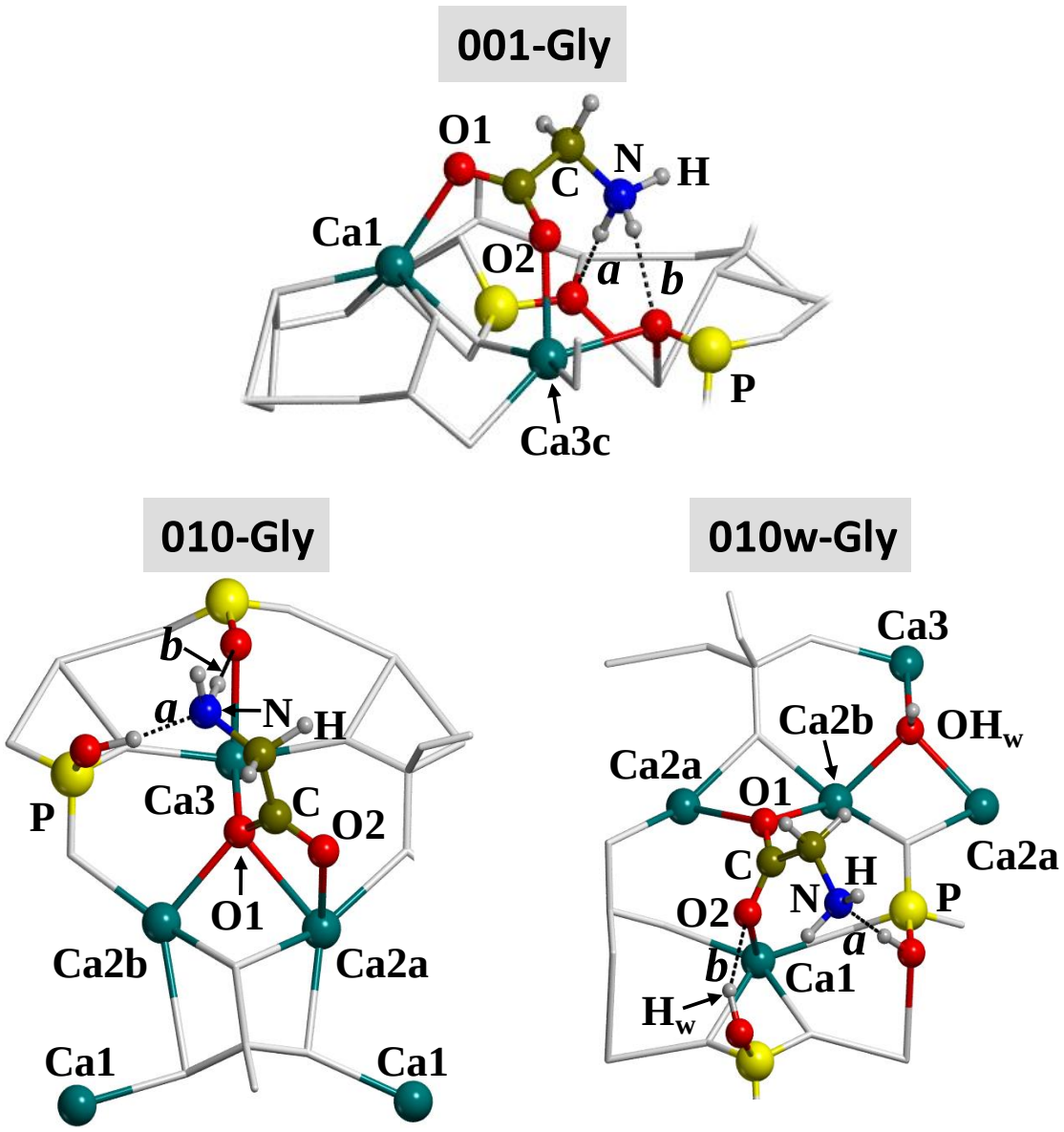
001-Gly
O1
C
N
H
Ca1
O2
a
b
P
Ca3c
010-Gly
b
a
N
H
P
Ca3
C
O2
O1
Ca2b
Ca2a
Ca1
Ca1
010w-Gly
Ca3
Ca2b
OHw
Ca2a
O1
Ca2a
C
H
N
P
O2
a
b
Ca1
Hw

Figure 2.

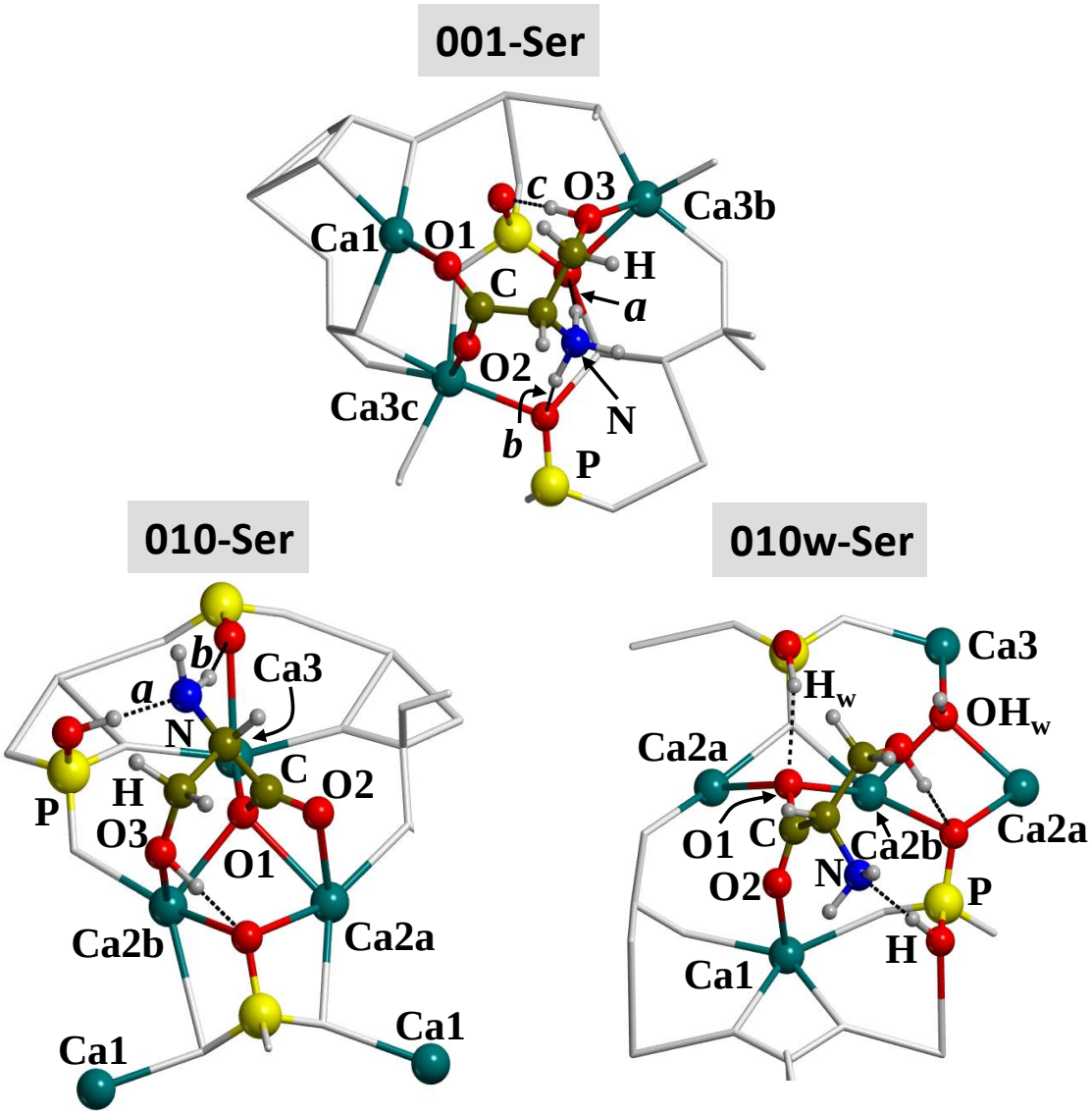
001-Ser
c
O3
Ca3b
Ca1
O1
H
C
a
O2
Ca3c
N
b
P
010-Ser
b
Ca3
a
N
C
O2
H
P
O3
O1
Ca2b
Ca2a
Ca1
Ca1
010w-Ser
Ca3
H$_w$
OH$_w$
Ca2a
O1
C
Ca2b
Ca2a
O2
N
P
H
Ca1

Figure 3.

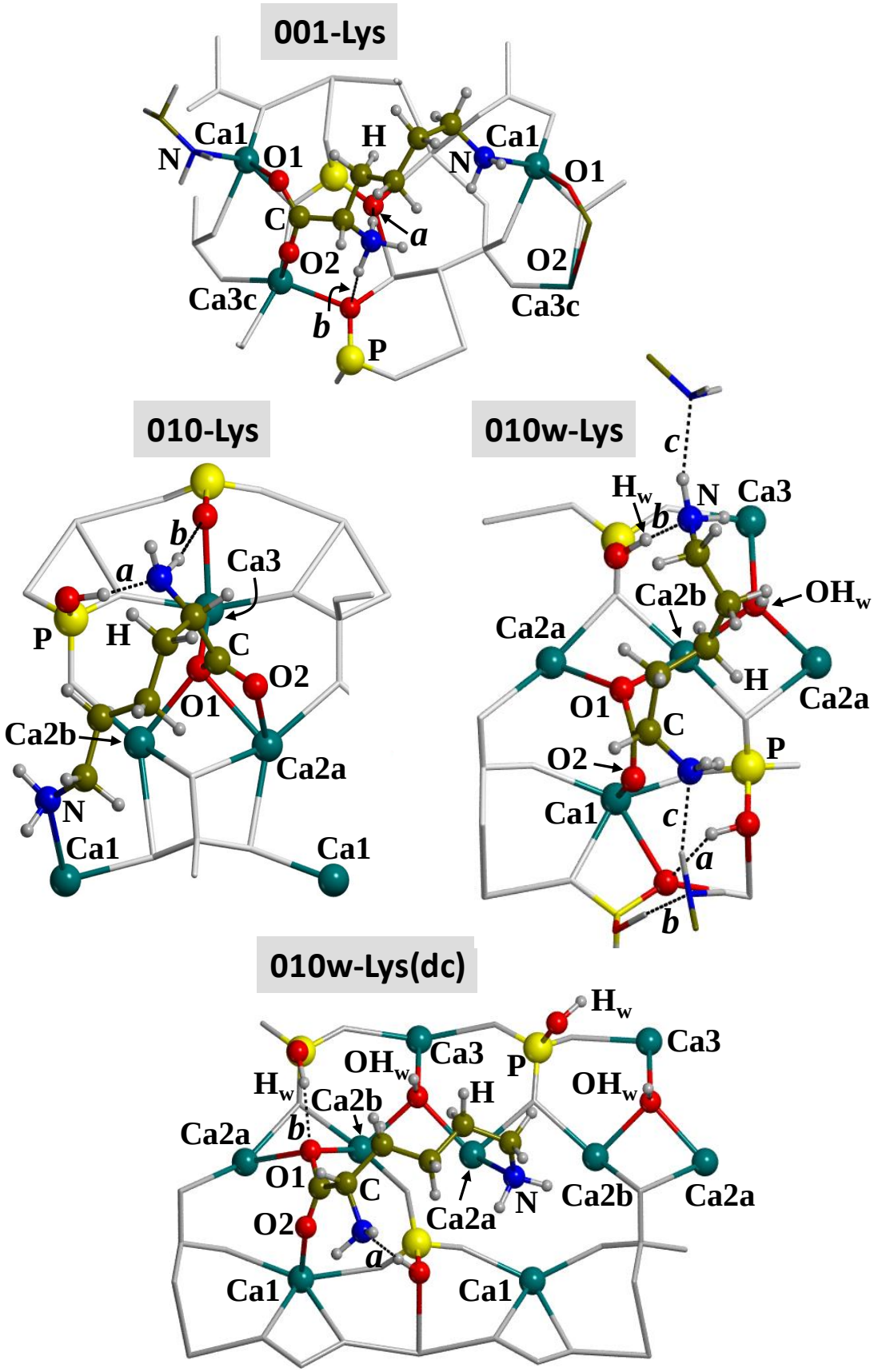
001-Lys
Ca1
N
O1
H
Ca1
N
O1
C
a
O2
O2
Ca3c
Ca3c
b
P
010-Lys
b
a
Ca3
P
H
C
O2
O1
Ca2b
Ca2a
N
Ca1
Ca1
010w-Lys
c
Hw
b
N
Ca3
Ca2b
OHw
Ca2a
H
Ca2a
O1
C
O2
P
Ca1
c
a
b
010w-Lys(dc)
Hw
OHw
Ca3
Ca3
P
OHw
Hw
Ca2b
H
Ca2a
b
O1
C
N
Ca2b
Ca2a
O2
Ca2a
a
Ca1
Ca1

Figure 4.

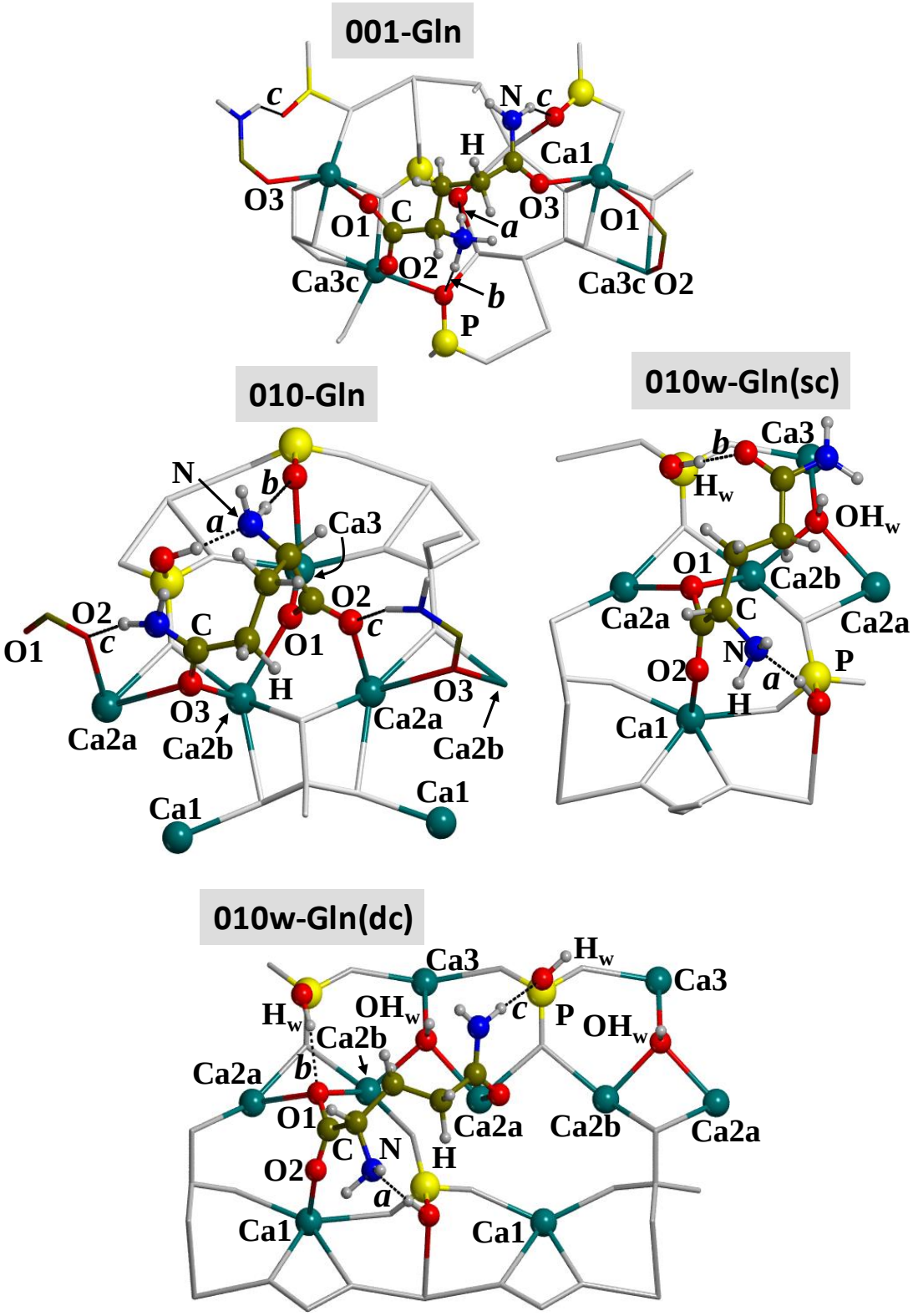
001-Gln
c
N
c
H
Ca1
O3
O1
C
O3
a
O1
O2
Ca3c
b
Ca3c
O2
P
010-Gln
N
b
a
Ca3
O2
O2
c
C
O1
c
O1
H
O3
O3
Ca2a
Ca2b
Ca2a
Ca2b
Ca1
Ca1
010w-Gln(sc)
b
Ca3
H$_w$
OH$_w$
O1
Ca2b
Ca2a
C
Ca2a
N
O2
P
a
H
Ca1
010w-Gln(dc)
Ca3
H$_w$
Ca3
H$_w$
OH$_w$
c
P
OH$_w$
Ca2b
Ca2a
b
O1
Ca2a
Ca2b
Ca2a
C
N
H
O2
a
Ca1
Ca1

Figure 5.

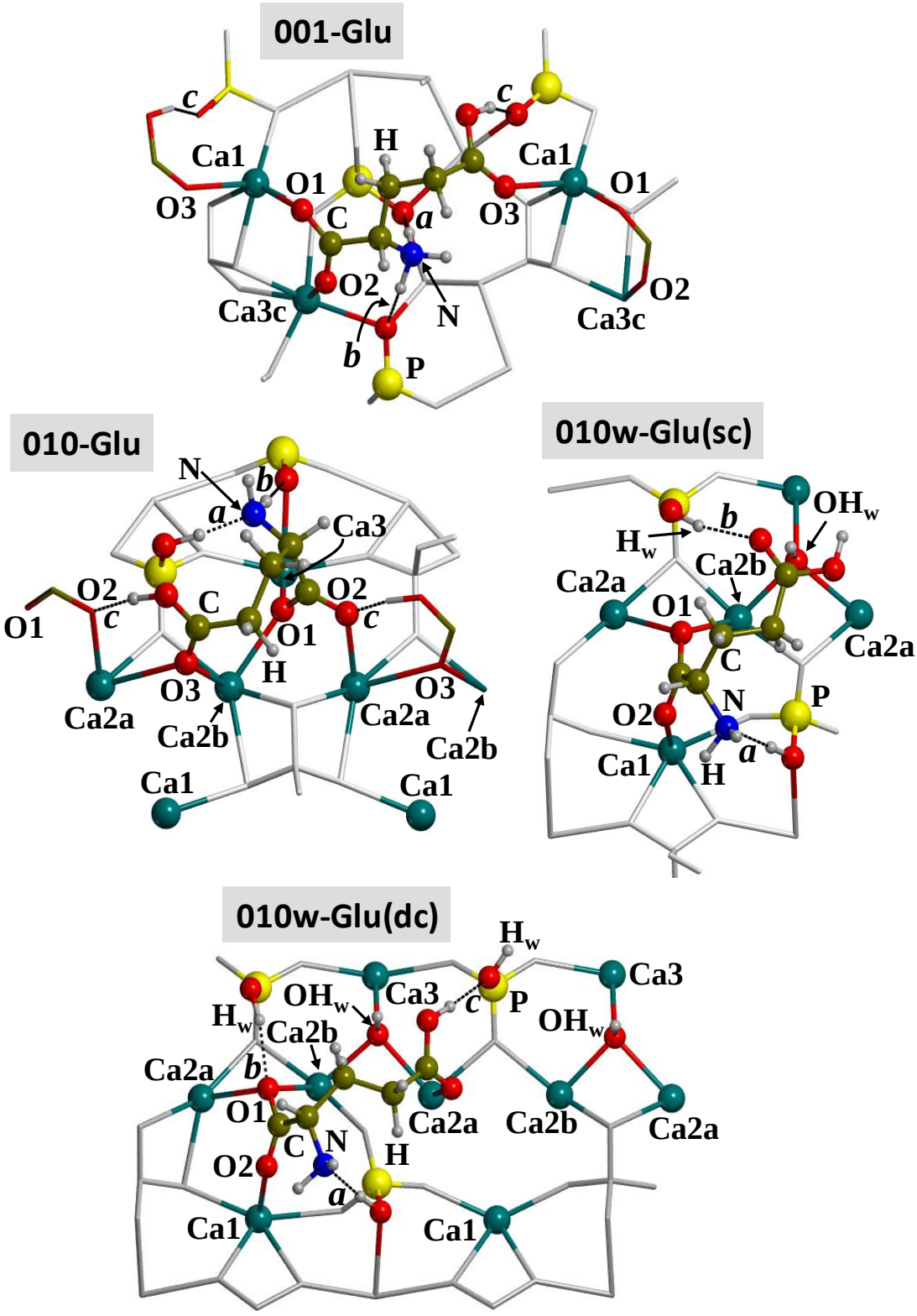
001-Glu
c
Ca1
O3
O1
H
C
a
O2
Ca3c
b
P
N
010-Glu
N
b
a
Ca3
O2
c
O1
C
O1
H
O3
Ca2a
Ca2b
Ca1
010w-Glu(sc)
OHw
b
Hw
Ca2b
Ca2a
O1
C
N
P
O2
Ca1
H
a
010w-Glu(dc)
Hw
Ca3
OHw
Ca3
c
P
Hw
Ca2b
OHw
Ca2a
b
O1
Ca2a
Ca2b
C
N
H
O2
a
Ca1

Figure 6.

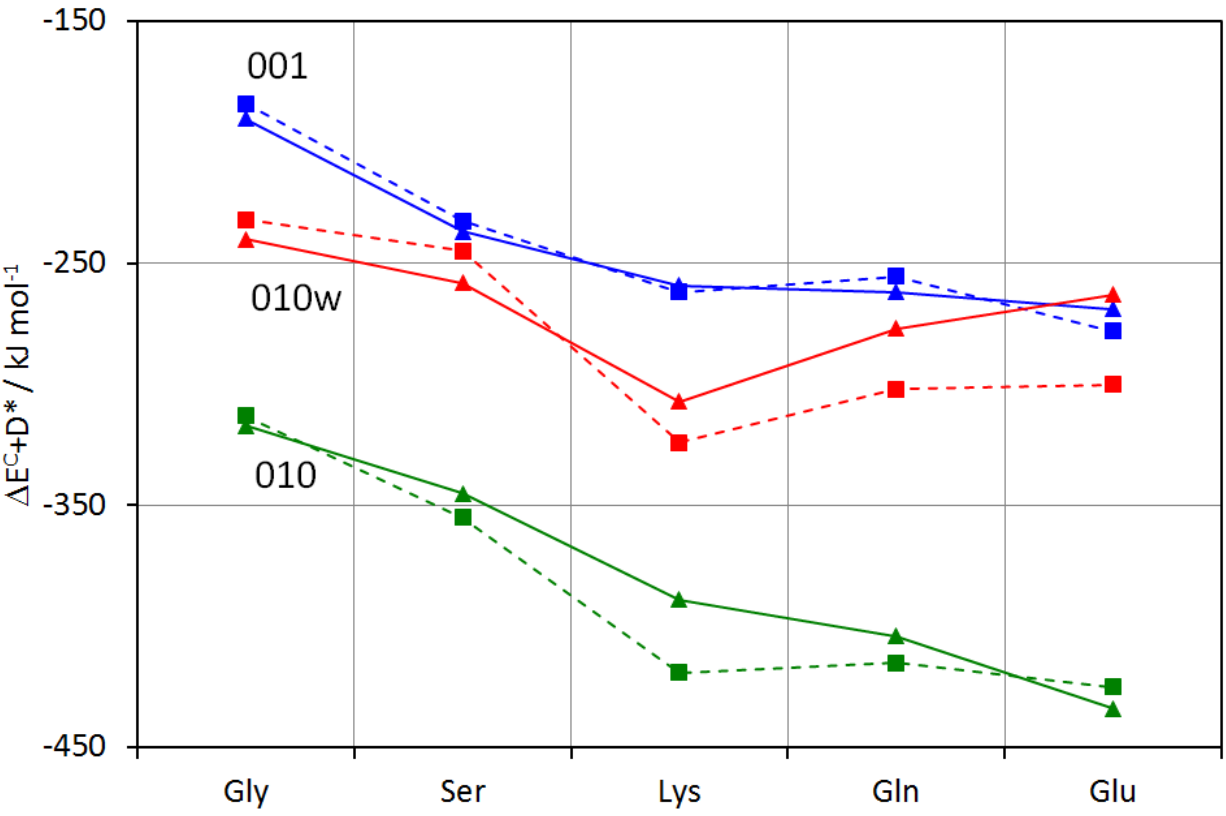

Figure 7.

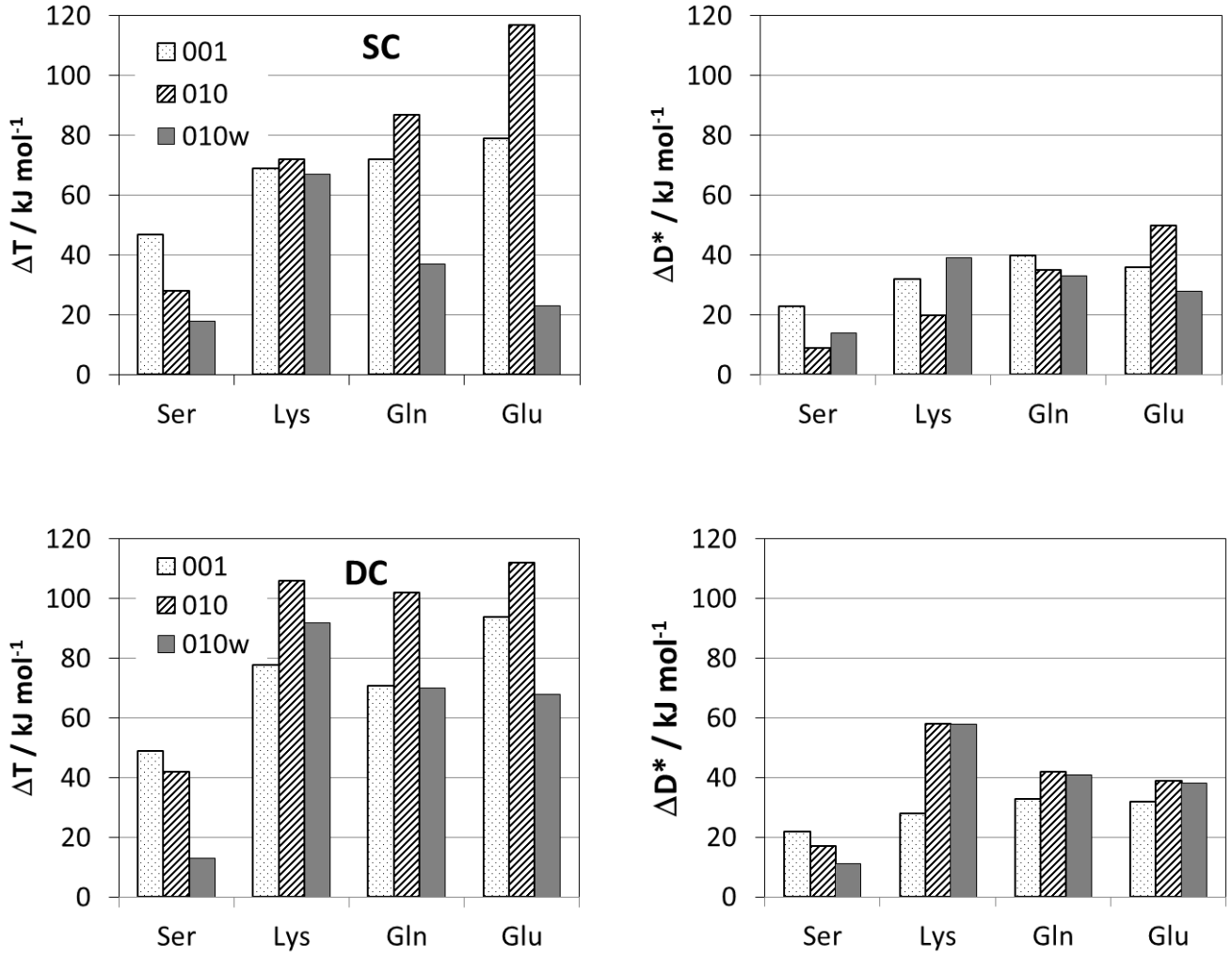
SC
001
010
010w
ΔT / kJ mol-1
ΔD* / kJ mol-1
120
100
80
60
40
20
0
Ser
Lys
Gln
Glu
DC
001
010
010w
ΔT / kJ mol-1
ΔD* / kJ mol-1
Ser
Lys
Gln
Glu

Figure 8.

References

(1) De, M., Ghosh, P. S. & Rotello, V. M. 2008 Applications of Nanoparticles in Biology. *Adv. Mater.* **20**, 4225-4241.
(2) Gray, J. J. 2004 The interaction of proteins with solid surfaces. *Curr. Opin. Struct. Biol.* **14**, 110-115.
(3) Hudson, S., Cooney, J. & Magner, E. 2008 Proteins in Mesoporous Silicates. *Angew. Chem. Int. Ed.* **47**, 8582-8594.
(4) Vallet-Regí, M., Balas, F. & Arcos, D. 2007 Mesoporous Materials for Drug Delivery. *Angew. Chem. Int. Ed.* **46**, 7548-7558.
(5) Vo-Dinh, T. 2007 *Nanotechnology in Biology and Medicine: Methods, Devices, and Applications*Taylor & Francis Group.
(6) Jones, F. H. 2001 Teeth and bones: applications of surface science to dental materials and related biomaterials. *Surf. Sci. Reports* **42**, 75-205.
(7) Ratner, B. D., Hoffman, A. S., Schoen, F. J. & Lemons, J. 2004 *Biomaterial Science: An Introduction to Materials in Medicine*Elsevier Inc.
(8) Hench, L. L. & Polak, J. M. 2002 Third-Generation Biomedical Materials. *Science* **295**, 1014-1017.
(9) LeGeros, R. Z. 2008 Calcium Phosphate-Based Osteoinductive Materials. *Chem. Rev.* **108**, 4742-4753.
(10) Palmer, L. C., Newcomb, C. J., Kaltz, S. R., Spoerke, E. D. & Stupp, S. I. 2008 Biomimetic Systems for Hydroxyapatite Mineralization Inspired By Bone and Enamel. *Chem. Rev.* **108**, 4754-4783.
(11) Hench, L. L., Splinter, R. J., Allen, W. C. & Greenlee, T. K. 1971 Bonding mechanisms at the interface of ceramic prosthetic materials. *J. Biomed. Mater. Res. Symp.* **2**, 117-141.
(12) Palazzo, B., Iafisco, M., Laforgia, M., Margiotta, N., Natile, G., Bianchi, C. L., Walsh, D., Mann, S. & Roveri, N. 2007 Biomimetic Hydroxyapatite–Drug Nanocrystals as Potential Bone Substitutes with Antitumor Drug Delivery Properties. *Adv. Funct. Mater.* **17**, 2180-2188.
(13) Morgan, T. T., Muddana, H. S., Altinoglu, E. Í., Rouse, S. M., Tabakovic, A., Tabouillot, T., Russin, T. J., Shanmugavelandy, S. S., Butler, P. J., Eklund, P. C.*et al.* 2008 Encapsulation of Organic Molecules in Calcium Phosphate Nanocomposite Particles for Intracellular Imaging and Drug Delivery. *Nano Lett.* **8**, 4108-4115.
(14) Shaw, W. J., Long, J. R., Dindot, J. L., Campbell, A. A., Stayton, P. S. & Drobny, G. P. 2000 Determination of Statherin N-Terminal Peptide Conformation on Hydroxyapatite Crystals. *J. Am. Chem. Soc.* **122**, 1709-1716.
(15) Long, J. R., Shaw, W. J., Stayton, P. S. & Drobny, G. P. 2001 Structure and Dynamics of Hydrated Statherin on Hydroxyapatite As Determined by Solid-State NMR. *Biochemistry* **40**, 15451-15455.
(16) Gibson, J. M., Popham, J. M., Raghunathan, V., Stayton, P. S. & Drobny, G. P. 2006 A Solid-State NMR Study of the Dynamics and Interactions of Phenylalanine Rings in a Statherin Fragment Bound to Hydroxyapatite Crystals. *J. Am. Chem. Soc.* **128**, 5364-5370.
(17) Goobes, R., Goobes, G., Campbell, C. T. & Stayton, P. S. 2006 Thermodynamics of Statherin Adsorption onto Hydroxyapatite. *Biochemistry* **45**, 5576-5586.

(18) Goobes, R., Goobes, G., Shaw, W. J., Drobny, G. P., Campbell, C. T. & Stayton, P. S. 2007 Thermodynamic Roles of Basic Amino Acids in Statherin Recognition of Hydroxyapatite. *Biochemistry* **46**, 4725-4733.
(19) Goobes, G., Goobes, R., Shaw, W. J., Gibson, J. M., Long, J. R., Raghunathan, V., Schueler-Furman, O., Popham, J. M., Baker, D., Campbell, C. T.*et al.* 2007 The structure, dynamics, and energetics of protein adsorption – lessons learned from adsorption of statherin to hydroxyapatite. *Magn. Reson. Chem.* **45**, S32-S47, and references therein.
(20) Chen, P.-H., Tseng, Y.-H., Mou, Y., Tsai, Y.-L., Guo, S.-M., Huang, S.-J., Yu, S. S.-F. & Chan, J. C. C. 2008 Adsorption of a Statherin Peptide Fragment on the Surface of Nanocrystallites of Hydroxyapatite. *J. Am. Chem. Soc.* **130**, 2862-2868.
(21) Kandori, K., Fudo, A. & Ishikawa, T. 2000 Adsorption of myoglobin onto various synthetic hydroxyapatite particles. *Phys. Chem. Chem. Phys.* **2**, 2015-2020.
(22) Kandori, K., Murata, K. & Ishikawa, T. 2007 Microcalorimetric Study of Protein Adsorption onto Calcium Hydroxyapatites. *Langmuir* **23**, 2064-2070.
(23) Shaw, W. J., Campbell, A. A., Paine, M. L. & Snead, M. L. 2004 The COOH Terminus of the Amelogenin, LRAP, Is Oriented Next to the Hydroxyapatite Surface. *J. Biol. Chem.* **279**, 40263-40266.
(24) Wallwork, M. L., Kirkham, J., Zhang, J., Smith, D. A., Brookes, S. J., Shore, R. C., Wood, S. R., Ryu, O. & Robinson, C. 2001 Binding of Matrix Proteins to Developing Enamel Crystals: An Atomic Force Microscopy Study. *Langmuir* **17**, 2508-2513.
(25) Kandori, K., Mukai, M., Yasukawa, A. & Ishikawa, T. 2000 Competitive and Cooperative Adsorptions of Bovine Serum Albumin and Lysozyme to Synthetic Calcium Hydroxyapatites. *Langmuir* **16**, 2301-2305.
(26) Brandes, N., Welzel, P. B., Werner, C. & Kroh, L. W. 2006 Adsorption-induced conformational changes of proteins onto ceramic particles: Differential scanning calorimetry and FTIR analysis. *J. Colloid Interface Sci.* **299**, 56-69.
(27) Elangovan, S., Margolis, H. C., Oppenheim, F. G. & Beniash, E. 2007 Conformational Changes in Salivary Proline-Rich Protein 1 upon Adsorption to Calcium Phosphate Crystals. *Langmuir* **23**, 11200-11205.
(28) Capriotti, L. A., Beebe, T. P., Jr. & Schneider, J. P. 2007 Hydroxyapatite Surface-Induced Peptide Folding. *J. Am. Chem. Soc.* **129**, 5281-5287.
(29) Chen, X., Wang, Q., Shen, J., Pan, H. & Wu, T. 2007 Adsorption of Leucine-Rich Amelogenin Protein on Hydroxyapatite (001) Surface through -COO- Claws. *J. Phys. Chem. C* **111**, 1284-1290.
(30) Makrodimitris, K., Masica, D. L., Kim, E. T. & Gray, J. J. 2007 Structure Prediction of Protein-Solid Surface Interactions Reveals a Molecular Recognition Motif of Statherin for Hydroxyapatite. *J. Am. Chem. Soc.* **129**, 13713-13722.
(31) Shen, J.-W., Wu, T., Wang, Q. & Pan, H.-H. 2008 Molecular simulation of protein adsorption and desorption on hydroxyapatite surfaces. *Biomaterials* **29**, 513-532.
(32) Pareek, A., Torrelles, X., Angermund, K., Rius, J., Magdans, U. & Gies, H. 2009 Competitive Adsorption of Glycine and Water on the Fluorapatite (100) Surface. *Langmuir* **25**, 1453-1458.
(33) Rosseeva, E. V., Golovanova, O. A. & Frank-Kamenetskaya, O. V. 2007 The Influence of Amino Acids on the Formation of Nanocrystalline Hydroxyapatite. *Glass Physics and Chemistry* **33**, 283-286.
(34) Shafei, G. M. S. E. & Moussa, N. A. 2001 Adsorption of Some Essential Amino Acids on Hydroxyapatite. *J. Colloid Interface Sci.* **238**, 160–166.

(35) Koutsopoulos, S. & Dalas, E. 2000 Hydroxyapatite crystallization in the presence of serine, tyrosine and hydroxyproline amino acids with polar side groups. *J. Crystal Growth* **216**, 443-449.
(36) Rimola, A., Corno, M., Zicovich-Wilson, C. & Ugliengo, P. 2008 Ab-initio Modelling of Protein/Biomaterial Interactions: Glycine Adsorption at Hydroxyapatite Surfaces. *J. Am. Chem. Soc.* **130**, 16181-16183.
(37) Rimola, A., Corno, M., Zicovich-Wilson, C. M. & Ugliengo, P. 2009 Ab initio modeling of protein/biomaterial interactions: competitive adsorption between glycine and water onto hydroxyapatite surfaces. *Phys. Chem. Chem. Phys.* **11**, 9005-9007.
(38) Gross, D. & Grodsky, G. 1955 On the Sublimation of Amino Acids and Peptides. *J. Am. Chem. Soc.* **77**, 1678-1680.
(39) Linder, R., Nispel, M., Häber, T. & Kleinermanns, K. 2005 Gas-phase FT-IR-spectra of natural amino acids. *Chem. Phys. Lett.* **409**, 260-264.
(40) Linder, R., Seefeld, K., Vavra, A. & Kleinermanns, K. 2008 Gas phase infrared spectra of nonaromatic amino acids. *Chem. Phys. Lett.* **453**, 1-6.
(41) Meng, M., Stievano, L. & Lambert, J. F. 2004 Adsorption and thermal condensation mechanisms of amino acids on oxide supports. 1. Glycine on silica. *Langmuir* **20**, 914-923.
(42) Rimola, A., Sakhno, Y., Bertinetti, L., Lelli, M., Martra, G. & Ugliengo, P. 2011 Toward a Surface Science Model for Biology: Glycine Adsorption on Nanohydroxyapatite with Well-Defined Surfaces. *J. Phys. Chem. Lett.* **2**, 1390-1394.
(43) Dovesi, R., Saunders, V. R., Roetti, C., Orlando, R., Zicovich-Wilson, C. M., Pascale, F., Civalleri, B., Doll, K., Harrison, N. M., Bush, I. J.*et al.* ; CRYSTAL06 User's Manual (University of Torino, Torino, 2006).
(44) Corno, M., Rimola, A., Bolis, V. & Ugliengo, P. 2010 Hydroxyapatite as a key biomaterial: quantum-mechanical simulation of its surfaces in interaction with biomolecules. *Phys. Chem. Chem. Phys.* **12**, 6309-6329.
(45) Becke, A. D. 1993 Density-functional thermochemistry. III. The role of exact exchange. *J. Chem. Phys.* **98**, 5648.
(46) Lee, C., Yang, W. & Parr, R. G. 1988 Development of the Colle-Slavetti correlation-energy formula into a functional of the electron density. *Phys. Rev. B* **37**, 785.
(47) Grimme, S. 2006 Semiempirical GGA-Type density functional constructed with a long-range dispersion correction. *J. Comp. Chem.* **27**, 1787-1799.
(48) Civalleri, B., Zicovich-Wilson, C. M., Valenzano, L. & Ugliengo, P. 2008 B3LYP augmented with an empirical dispersion term (B3LYP-D*) as applied to molecular crystals. *CrystEngComm* **10**, 405-410.
(49) Corno, M., Busco, C., Civalleri, B. & Ugliengo, P. 2006 Periodic ab initio study of structural and vibrational features of hexagonal hydroxyapatite Ca10(PO4)6(OH)2. *Phys. Chem. Chem. Phys.* **8**, 2464-2472.
(50) Corno, M., Orlando, R., Civalleri, B. & Ugliengo, P. 2007 Periodic B3LYP study of hydroxyapatite (001) surface modelled by thin layer slabs. *Eur. J. Mineral.* **19**, 757-767.
(51) Corno, M., Busco, C., Bolis, V., Tosoni, S. & Ugliengo, P. 2009 Water Adsorption on the Stoichiometric (001) and (010) Surfaces of Hydroxyapatite: A Periodic B3LYP Study. *Langmuir* **25**, 2188-2198.
(52) Mkhonto, D. & de Leeuw, N. H. 2002 A computer modelling study of the effect of water on the surface structure and morphology of fluorapatite: introducing a $Ca_{10}(PO_4)_6F_2$ potential model. *J. Mater. Chem.* **12**, 2633-2642.

(53) de Leeuw, N. H. & Rabone, J. A. L. 2007 Molecular dynamics simulations of the interaction of citric acid with the hydroxyapatite (0001) and (011¯0) surfaces in an aqueous environment. *CrystEngComm* **9**, 1178-1186.
(54) Vallet-Regí, M. & González-Calbet, J. M. 2004 Calcium phosphates as substitution of bone tissues. *Progress in Solid State Chemistry* **32**, 1-31.
(55) Simmer, J. P. & Fincham, A. G. 1995 Molecular mechanisms of dental enamel formation. *Crit. Rev. Oral Biol. Med.* **6**, 84-108.
(56) Kirkham, J., Brookes, S. J., Shore, R. C., Wood, S. R., Smith, D. A., Zhang, J., Chen, H. & Robinson, C. 2002 Physico-chemical properties of crystal surfaces in matrix–mineral interactions during mammalian biomineralisation. *Curr. Opin. Colloid Interface Sci.* **7**, 124-132.
(57) Sato, K., Kogure, T., Iwai, H. & Tanaka, J. 2002 Atomic-Scale {101¯0} Interfacial Structure in Hydroxyapatite Determined by High-Resolution Transmission Electron Microscopy (p 3054-3058). *J. Am. Ceram. Soc.* **85**, 3054-3058.
(58) Astala, R. & Stott, M. J. 2008 First-principles study of hydroxyapatite surfaces and water adsorption. *Phys. Rev. B* **78**, 075427.
(59) Almora-Barrios, N., Austen, K. F. & de Leeuw, N. H. 2009 Density Functional Theory Study of the Binding of Glycine, Proline, and Hydroxyproline to the Hydroxyapatite (0001) and (010) Surfaces. *Langmuir* **25**, 5018-5025.
(60) Corral, I., Mó, O., Yáñez, M., Salpin, J.-Y., Tortajada, J., Morán, D. & Radom, L. 2006 An Experimental and Theoretical Investigation of Gas-Phase Reactions of Ca2+ with Glycine. *Chem. Eur. J.* **12**, 6787-6796.
(61) Filgueiras, M. R. T., Mkhonto, D. & de Leeuw, N. H. 2006 Computer simulations of the adsorption of citric acid at hydroxyapatite surfaces. *J. Crystal Growth* **294**, 60-68.